IPPI

Polyolefins Journal, Vol. 2 No. 2 (2015) 65-71

ORIGINAl PAPER

Addition of a second alcohol in magnesium ethoxide synthesis as a way to vary the pore architecture of Ziegler-Natta catalysts

Toshiaki Funako, Patchanee Chammingkwan, Toshiaki Taniike, Minoru Terano*

School of Materials Science, Japan Advanced Institute of Science and Technology, 1-1 Asahidai, Nomi, Ishikawa 923-1292, Japan

Received: 13 January 2015, Accepted: 24 January 2015

ABSTRACT

In Ziegler-Natta olefin polymerization, the pore architecture of catalysts plays a crucial role in catalytic performances and polymer properties. While the type of preparation routes (such as chemical reaction and solution precipitation) greatly affects the catalyst pore architecture as a result of different solidification mechanisms, the modification of the pore architecture within a given route has been hardly achieved. In this study, we propose a simple way to vary the pore architecture of $Mg(OEt)_2$-based Ziegler-Natta catalysts by the addition of a second alcohol. It was found that the addition of a second alcohol during $Mg(OEt)_2$ synthesis affected not only the morphology of $Mg(OEt)_2$ macroparticles but also the shape of building units. The degree of alternation was found to be sensitive to the molecular structure of a second alcohol. Noticeable influences were observed in the case of branched alcohols, where the transformation of plate-like building units to cylindrical ones led to the generation of totally different pore size distributions of resultant catalysts. **Polyolefins J (2015) 2: 65-71**

Keywords: Ziegler-Natta catalysts; pore architecture; magnesium alkoxide

INTRODUCTION

Polyolefins are commodity thermoplastics mainly made from polymerization of olefins. They have been used in an enormous amount for a variety of applications because of their excellent properties at a relatively low production cost. Improvements in the production efficiency and material properties have been pursued to respond to the continuingly expanding demands and applications. From such a point of view, rational catalyst design is essential.

Ziegler-Natta catalysts, comprising of $MgCl_2$-supported $TiCl_4$ and a Lewis basic compound, are one of the most important olefin polymerization catalysts [1]. Nowadays, most of industrial catalysts are synthesized in two major routes: One is a precipitation route via alcohol adducts of $MgCl_2$[2,3] and the other is a chemical reaction method using magnesium ethoxide ($Mg(OEt)_2$) as a precursor [4,5]. Both types of catalysts basically provide excellent performances in industrial olefin polymerization. However, it is also known that

* Corresponding Author - E-mail: terano@jaist.ac.jp

these two types of catalysts exhibit quite different catalytic behaviors [6], and such details are critical for the advanced control. In the precipitation method, solid catalysts are precipitated from $MgCl_2$ alcohol solution. Resultant catalyst particles are typically formed by agglomeration of smaller spheroidal sub-particles to yield grape-like morphology [3]. The control of the particle size and morphology is prudently done by the control of the reaction rate and shear force in the precipitation. On the contrary, the chemical conversion technique utilizes pre-formed spherical $Mg(OEt)_2$ particles and converts them into catalysts by chlorination. The morphology of resultant catalysts mimics that of original $Mg(OEt)_2$ particles that are made by agglomeration of plate-like sub-particles [7]. These differences in the particle formulation allow the two types of catalysts to equip specific pore architectures, which greatly differentiate their catalytic behaviors in terms of morphological control [8], kinetics [9], comonomer incorporation efficiency [10], and so on.

In spite of the said tremendous importance, a method to systematically control the pore architecture of Ziegler-Natta catalysts has not been yet established. Difficulties are mainly attributed to the following reasons:

i) Due to the complicated hierarchical structure of catalyst particles, it is not easy to identify and quantify the pore architecture. Consequently, most of catalyst developments have been conducted in a highly empirical manner without analyzing the pore architecture.
ii) While the two major preparation routes endow quite different pore architectures, the variation of reaction conditions in each specific route hardly alters the pore architecture.

For the former issue, we have recently reported a way to quantify the pore architecture of Ziegler-Natta catalysts as a part of our efforts in establishing catalyst structure-performance relationships [11-13]. Here, we disclose a novel but simple strategy to alter the pore architecture of $Mg(OEt)_2$-based Ziegler-Natta catalysts. We found that the pore architecture of catalysts, which is hardly affected by reaction conditions, is effectively altered by the co-existence of a second alcohol during $Mg(OEt)_2$ synthesis.

EXPERIMENTAL

Material

Mg powder was donated by Yuki Kogyo Co., Ltd. The mean particle size (D_{50}) and particle size distribution ($(D_{90}$-$D_{10})/D_{50}$) of the Mg powder were 17.2 μm and 1.78, respectively. Methanol (purity > 99.5%), ethanol (purity > 99.5%), *n*-propanol (purity > 99%) and *i*-propanol (purity > 99%) were dried over 3A molecular sieves followed by N_2 bubbling. Four kinds of butanol isomers (purity > 98%), *n*-heptane (purity > 99.5%), toluene (purity > 99.5%) and di-*n*-butylphthalate (DBP) (purity > 98%) were dried over 4A molecular sieves with N_2 bubbling. I_2 (purity > 99%) and $TiCl_4$ (purity > 99%) were used as received.

$Mg(OR)_2$ synthesis

Eight $Mg(OR)_2$ samples were synthesized by reacting the Mg powder with ethanol/second alcohol mixture. According to the employed second alcohol, the samples are denoted as MGR-Et, MGR-Me, MGR-*n*Pr, MGR-*i*Pr, MGR-*n*Bu, MGR-*i*Bu, MGR-*s*Bu and MGR-*t*Bu. The details are summarized in Table 1. All the samples were synthesized based on the following procedure. 0.67 g of I_2 and 32 mL of alcohol mixture were introduced into a jacket-type glass reactor equipped with a mechanical stirrer rotating at 180 rpm. After the dissolution of I_2 at 75°C, 2.5 g of Mg and 32 mL of alcohol mixture were introduced five times with the time interval of 10 min. After the fifth addition, the reaction suspension was aged at 75°C for 2 h under stirring. The obtained $Mg(OR)_2$ was washed with the corresponding alcohol mixture and dried by a rotary evaporator.

Catalyst preparation

Ziegler-Natta catalysts were prepared from synthe-

Table 1. $Mg(OR)_2$ sample information.

Sample	Second alcohol	Ratio (mol%)	
		Ethanol	Second alcohol
MGR-Et	-	100	-
MGR-Me	methanol	95	5.0
MGR-*n*Pr	*n*-propanol	95	5.0
MGR-*i*Pr	*i*-propanol	95	5.0
MGR-*n*Bu	*n*-butanol	95	5.0
MGR-*i*Bu	*i*-butanol	90	10
MGR-*s*Bu	*s*-butanol	90	10
MGR-*t*Bu	*t*-butanol	90	10

sized $Mg(OR)_2$ based on a previously reported procedure [11]. 15 g of $Mg(OR)_2$ and 150 mL of toluene were introduced into 500 mL of a three neck flask under N_2 atmosphere and the suspension was cooled down to 0°C. 30 mL of $TiCl_4$ was dropwise added to the suspension, during which the temperature was kept below 5°C. Thereafter, the temperature of the suspension was once raised to 90°C to add 4.5 mL of DBP, followed by heating at 110°C for 2 h. The suspension was washed twice by decantation using toluene at 90°C and further chlorination was carried out using 30 mL of $TiCl_4$ at 110°C for 2 h. Catalyst samples were obtained after repetitive washing of solid particles with *n*-heptane. Eight catalyst samples, denoted as Cat-Et, Cat-Me, Cat-*n*Pr, Cat-*i*Pr, Cat-*n*Bu, Cat-*i*Bu, Cat-*s*Bu, and Cat-*t*Bu, were respectively prepared from the corresponding $Mg(OR)_2$ samples.

Characterization

Morphological characteristics of $Mg(OR)_2$ and catalyst particles were studied by scanning electron microscopy (SEM, Hitachi S-4100) operated at an accelerating voltage of 20 kV. All the samples were prepared under N_2 atmosphere and subjected to Pt/Pd sputtering for 100 s before the measurement. Pore architectures of catalyst samples were analyzed by N_2 adsorption/desorption measurements at 77 K by a BELSORP-max instrument (BEL JAPAN, INC.). The samples were out-gassed at 80°C for 3 h in vacuum prior to the measurements. The micropore volume with the dimension below 2 nm (V_{micro}, $D< 2$ nm) was derived based on an equation that had been proposed in our previous literature [11]. The mesopore volume (V_{meso}, $2 <D< 50$ nm) was derived based on either the BJH or the INNES method: The former is suitable for cylindrical porosity and the latter for slit-shaped porosity [14-15]. The macropore volume (V_{macro}, $D> 50$ nm) was also estimated from the extent of unrestricted sorption (described later).

RESULTS AND DISCUSSIONS

Eight $Mg(OR)_2$ samples were synthesized according to the alcohol composition given in Table 1. The morphological characteristics of the $Mg(OR)_2$ particles were observed by SEM (Figure 1). The standard sample (MGR-Et, Figure 1a,b), which was synthesized from pure ethanol, possessed a spherical shape, whose size (D_{50}) and size distribution ($(D_{90}-D_{10})/D_{50}$) were determined as 21.7 μm and 0.52, respectively [11]. A high-magnification image revealed that the particles were composed by agglomeration of plate-like building blocks, whose lateral dimension varied in the range of 500-1000 nm with the plate thickness of about 100 nm. The inclusion of a second alcohol in $Mg(OEt)_2$ around 5 mol% significantly distorted the particle shape. The inclusion of methanol (MGR-Me, Figure 1c,d) led to secondary agglomeration of a few particles to distort the shape of macroparticles. The lateral size of building blocks became substantially larger compared to MGR-Et, while the plate thickness was slightly increased to about 150 nm. MGR-*n*Pr, which was synthesized in the presence of 5 mol% *n*-propanol, maintained the basic $Mg(OEt)_2$ structures, although the particle size distributions became much broader due to the formation of smaller particles (Figure 1e,f). By changing the constitutional isomers from *n*-propanol to *i*-propanol (Figure 1g,h), the particle size distribution drastically improved and the size of particles became similar to that of MGR-Et. However, the magnified image clarified that the building blocks were not anymore similar to those of MGR-Et: MGR-*i*Pr particles consisted of distorted cylindrical building blocks rather than plate-like ones. The longer dimension of the distorted cylindrical building blocks was in the range of 400-700 nm with the shorter dimension around 300 nm. The inclusion of *n*-butanol, *i*-butanol, and *s*-butanol led to similar shapeless morphologies without distinguishable building blocks (Figure 1i-n). Judging from smooth surfaces as well as severely fused sub-particles, it was believed that these butanol isomers prevented the crystallization of $Mg(OR)_2$. Only *t*-butanol formed well-distinguishable particles. However, the particle surfaces became much rougher compared to MGR-Et due to much thicker building blocks (Figure 1o,p). All of these results emphasized that the particle and building block morphologies of $Mg(OR)_2$ are extremely sensitive to the presence of different kinds of alcohols even at a small proportion (5-10 mol%). Although the reaction was carried out in the predominantly excess molar ratio of ethanol, a second alcohol more or less competitively reacted and incorporated into the $Mg(OR)_2$ structure to some extent, which evidently affected the formation/growth mechanisms of the particles and building blocks. As was proposed by Tanase et al. [16], the reaction between

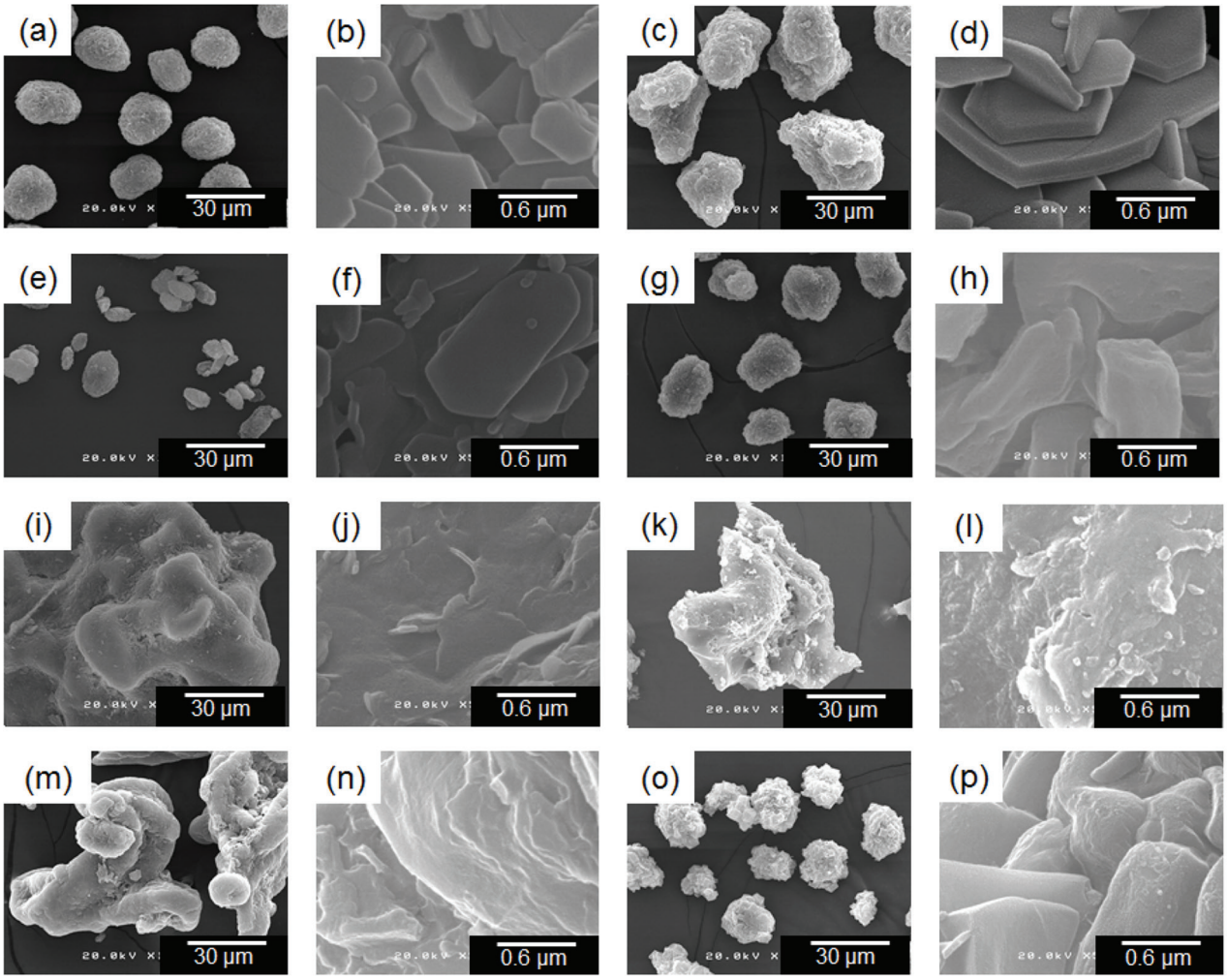

Figure 1. SEM images of $Mg(OR)_2$ particles: (a,b) MGR-Et (x1000, x50000), (c,d) MGR-Me (x1000, x50000), (e,f) MGR-*n*Pr (x1000, x50000), (g,h) MGR-*i*Pr (x1000, x50000), (i,j) MGR-*n*Bu (x1000, x50000), (k,l) MGR-*i*Bu (x1000, x50000), (m,n) MGR-*s*Bu (x1000, x50000), and (o,p) MGR-*t*Bu (x1000, x50000).

metallic Mg and ethanol with the aid of I_2 goes through repetitive dissolution and precipitation via an intermediate state expressed as $nMg(OEt)_2 \bullet MgI_2 \bullet mEtOH$ to form plate-like $Mg(OEt)_2$ precipitates on Mg surfaces. These plate-like seeds exfoliate from Mg surfaces and grow into macroparticles. Hence, the inclusion of a second alcohol with different structures was believed to greatly influence the dissolution and precipitation equilibrium (though the relationship with the molecular structure of a second alcohol was yet unclear).

The $Mg(OR)_2$ samples were converted into catalysts under the same preparation condition. Catalyst particle morphologies were observed by SEM. The results are shown in Figure 2. The particle shape and size of Cat-Et well replicated those of MGR-Et (Figure 2a). Such morphological replication is quite usual as long as original particles are not fragile [11]. While Cat-Me and Cat-*i*Pr more or less maintained the original particle morphologies (Figure 2b,d), Cat-*n*Pr exhibited a plenty of fine particles (Figure 2c). This fact indicated that the MGE-*n*Pr particles were fragile enough to be disintegrated during the chlorination process. When the shapeless MGE-*n*Bu and MGE-*i*Bu particles were employed for the catalyzation, a peculiar phenomenon was observed: Even though the original particles were shapeless and huge (> 50 μm), the catalyst particles were roughly spheroidal with the size around 25~35 μm (Figure 2e,f). It was speculated that the original shapeless particles broke up into sub-particles, and these sub-particles were more or less shaped into the spheroidal morphology in the chlorination. In the case of Cat-*t*Bu, cracks were observed on the particles (Figure 2h).

Pore architectures of the catalyst samples were characterized based on the N_2 adsorption/desorption measurements. The isotherms for all the samples are

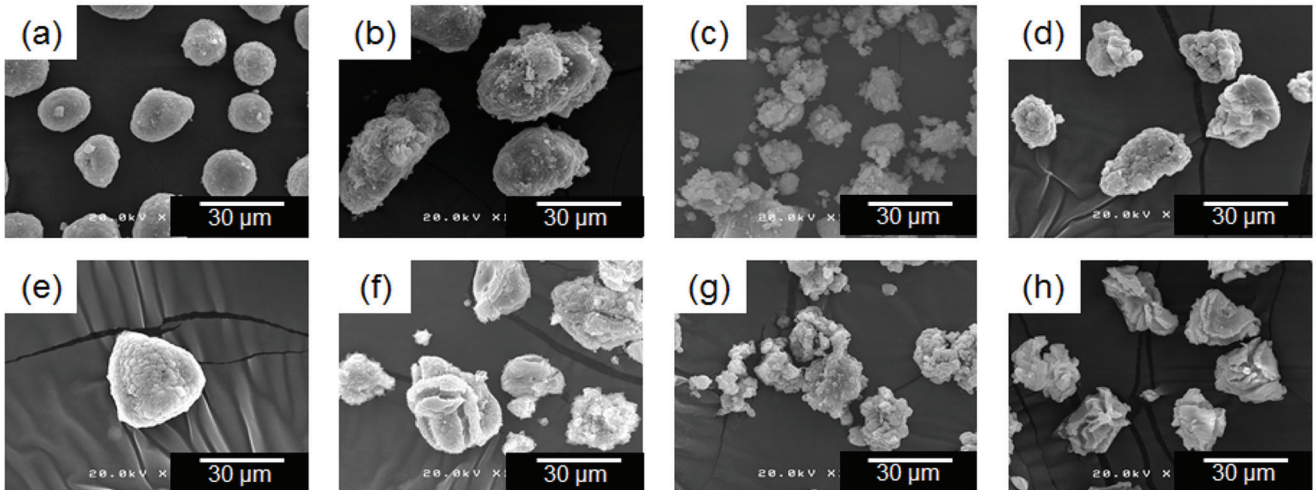

Figure 2. SEM images of catalyst particles (x1000): (a) Cat-Et, (b) Cat-Me, (c) Cat-*n*Pr, (d) Cat-*i*Pr, (e) Cat-*n*Bu, (f) Cat-*i*Bu, (g) Cat-*s*Bu, and (h) Cat-*t*Bu.

shown in Figure 3, while the classification and analysis results are summarized in Table 2. The N_2 uptake for Cat-Et rapidly increased at low relative pressure (p/p_0=0-0.1) followed by successive increments. Featured with a relatively great extent of unrestricted sorption at high relative pressure (p/p_0>0.98), the isotherm was assigned as the type II of the IUPAC classification for macroporous or non-porous materials.

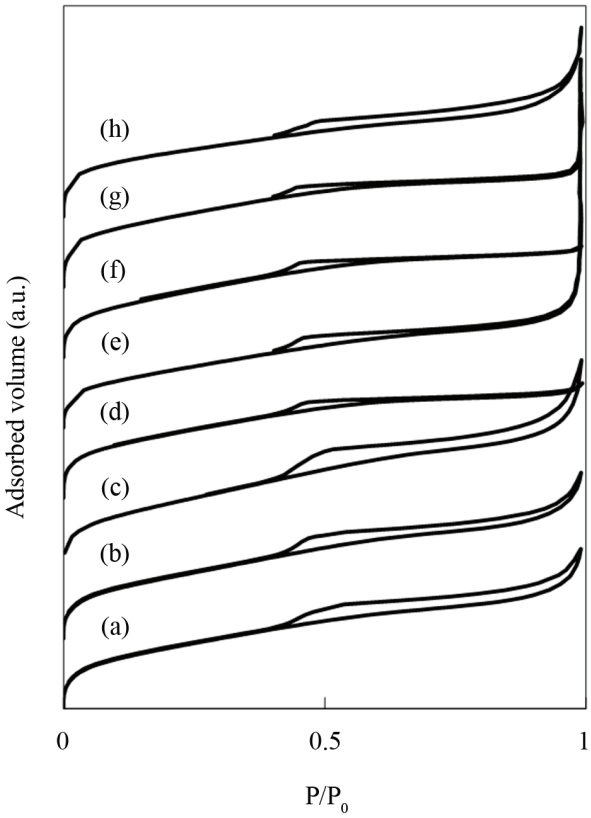

Figure 3. N_2 adsorption/desorption isotherms for catalyst samples: (a) Cat-Et, (b) Cat-Me, (c) Cat-*n*Pr, (d) Cat-*i*Pr, (e) Cat-*n*Bu, (f) Cat-*i*Bu, (g) Cat-*s*Bu, and (h) Cat-*t*Bu.

The hysteresis loop made by the adsorption and desorption isotherms at the mesopore region belonged to the type H3, suggesting the capillary condensation in slit-shaped mesopores, whose sizes and shapes are non-uniform [17,18]. The isotherms for Cat-Me, Cat-*n*Pr and Cat-*t*Bu were quite similar to those for Cat-Et (i.e. the adsorption isotherm of the type II and the hysteresis of the type H3). It had been concluded in our previous literature that plate-like building blocks lead to the formation of slit-shaped mesopores, while cylindrical building blocks form cylindrical mesopores [17,18]. In actual, Cat-Et, Cat-Me and Cat-*n*Pr showed slit-shaped mesopores as a result of their plate-like building blocks (see Figure 1). The adsorption isotherms for Cat-*i*Pr and Cat-*i*Bu belonged to the type I for microporous materials, since the N_2 uptake occurred mainly at low relative pressure with only small uptakes in the mesopore and unrestricted-sorption regions. Their hysteresis loops were categorized into the type H2, corresponding to cylindrical mesopores with non-uniform sizes and shapes. This fact was consistent with the cylindrical building blocks for MGE-*i*Pr (while building blocks were not clearly observed for MGE-*i*Bu). Cat-*n*Bu and Cat-*s*Bu similarly exhibited the hysteresis of the type H2 with a larger portion of N_2 uptake at high relative pressure, suggesting that a great amount of macropores or interparticle voids were formed due to particle disintegration in the chlorination.

The pore volume was calculated from the N_2 adsorption/desorption isotherms. Since relatively well-known methods such as HK [19] and SF [20] are not applicable to Ziegler-Natta catalysts, the micropore

Table 2. Summary of N_2 adsorption/desorption isotherms.

Sample	Classification		Pore shape	Pore volume (mm^3g^{-1})		
	Isotherm	Hysteresis		V_{micro}	V_{meso}	V_{macro} [(a)]
Cat-Et	II	H3	slit	107	180	medium
Cat-Me	II	H3	slit	108	188	medium
Cat-*n*Pr	II	H3	slit	107	233	large
Cat-*i*Pr	I	H2	cylinder	153	65	small
Cat-*n*Bu	II	H2	cylinder	140	144	large
Cat-*i*Bu	I	H2	cylinder	163	55	small
Cat-*s*Bu	II	H2	cylinder	179	65	large
Cat-*t*Bu	II	H3	slit	143	200	large

[(a)] Estimated from the extent of unrestricted sorption.

volume was calculated based on the equation proposed by us [11, 21]. The analysis method for the mesopore volume was chosen either from the BJH or INNES method according to the above-determined pore shape characteristics. In a typical relative pressure range (p/p_0=0-0.98), the N_2 condensation never occurs in macropores, i.e. the macropore volume is not available. However, it is possible to roughly estimate the macropore volume from the extent of unrestricted sorption over p/p_0=0.98.

Thus derived pore volume information is given in Table 2 and Figure 4. The pore volume distributions were classified into two types. The first type (Cat-Et, Cat-Me, Cat-*n*Pr, Cat-*n*Bu and Cat-*t*Bu) was associated with a wide range of porosity with a bimodal distribution centered at $D < 2$ nm (micropores) and 20 nm $\leq D \leq$ 50 nm (large mesopores), which is usual for $Mg(OEt)_2$-based Ziegler-Natta catalysts. The second type (Cat-*i*Pr, Cat-*i*Bu and Cat-*s*Bu) presented the dominance of micropore volume with diminishing pore volume at a larger pore dimension. Interestingly, the classification of the pore volume distributions was synchronized with that of the hysteresis: Catalysts with slit-shaped mesopores led to the bimodal distribution, while cylindrical mesopores led to the micropore dominance. Since the pore shape was determined by the shape of the building blocks (pores are interspaces between stacked building blocks), different pore volume distributions could be tracked back to the difference in the building block shape, which was sensitively affected by the presence of a second alcohol. In other words, the addition of a second alcohol could be regarded as a way to engineer the catalyst porosity.

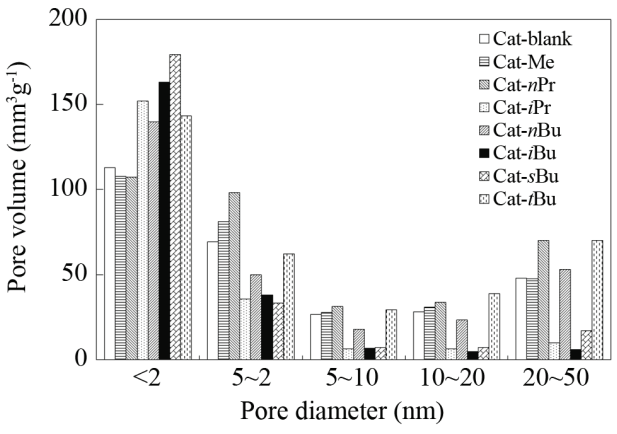

Figure 4. Pore size distributions for catalyst samples.

CONCLUSION

In this study, $Mg(OR)_2$ samples as precursor particles for Zielger-Natta catalysts were prepared by mixing a small amount of different second alcohols in the reaction between metallic Mg and ethanol. The resultant influences were studied on the particle and pore characteristics of Ziegler-Natta catalysts. It was found that the particle morphologies were extremely sensitive to the molecular structure of the second alcohol. Second alcohols altered not only the macroparticle size and shape but also the shape of the building blocks, probably through the dissolution/precipitation equilibrium in the $Mg(OR)_2$ formation. The alternation of the building block shapes resulted in the generation of different pore volume distributions, which is expected to be useful for engineering the pore architecture of Ziegler-Natta catalysts. Further studies are required to clarify mechanistic aspects how a second alcohol modulates the particle formation of $Mg(OR)_2$.

REFERENCES

1. Soga K, Shiono T (1997) Ziegler-Natta catalysts for olefin polymerizations. Prog Polym Sci 22:

1503-1546
2. Hadian N, Hakim S, Nekoomanesh-Haghighi M, Bahri-Laleh N (2014) Storage time effect on dynamic structure of $MgCl_2$.nEtOH adducts in heterogeneous Ziegler-Natta catalysts. Polyolefins J 1: 33-41
3. Dil EJ, Pourmahdian S, Vatankhah M, Afshar Taromi F (2010) Effect of dealcoholation of support in $MgCl_2$-supported Ziegler–Natta catalysts on catalyst activity and polypropylene powder morphology. Polym Bull 64: 445-457
4. Terano M, Murai A, Inoue M, Miyosi K (1987) JP1987158704 (to Toho Catalyst Co. Ltd.)
5. Nitta T, Liu B, Nakatani H, Terano M (2002) Formation, deactivation and transformation of stereospecific active sites on $TiCl_4$/dibutylphthalate/$Mg(OEt)_2$ catalyst induced by short time reaction with Al-alkyl cocatalyst. J Mol Catal A: Chem 180: 25-34
6. Pokasermsong P, Praserthdam P (2009) Comparison of activity of Ziegler-Natta catalysts prepared by recrystallization and chemical reaction methods towards polymerization of ethylene. Eng J 13: 57-64
7. Tanase S, Katayama K, Inasawa S, Okada F, Yamaguchi Y, Sadashima T, Yabunouchi N, Konakazawa T, Junke T, Ishihara N (2008) New synthesis method using magnesium alkoxides as carrier materials for Ziegler-Natta catalysts with spherical morphology. Macromol React Eng 2: 233-239
8. Zheng X, Pimplapure MS, Weickert G, Loos J (2006) Influence of copolymerization on fragmentation behavior using Ziegler-Natta catalysts. Macromol Rapid Commun 27: 15-20
9. Dashti A, Ramazani SA, Hiraoka Y, Kim SY, Taniike T, Terano M (2009) Kinetic and morphological study of a magnesium ethoxide-based Ziegler–Natta catalyst for propylene polymerization. Polym Int 58: 40-45
10. Ko YS, Woo SI (2003) Shape and diffusion of the monomer-controlled copolymerization of ethylene and α-olefins over Cp_2ZrCl_2 confined in the nanospace of the supercage of NaY. J Polym Sci A: Polym Chem 41: 2171-2179
11. Taniike T, Funako T, Terano M (2014) Multilateral characterization for industrial Ziegler–Natta catalysts toward elucidation of structure-performance relationship. J Catal 311: 33-40
12. Chammingkwan P, Thang VQ, Terano M, Taniike T (2014) MgO/$MgCl_2$/$TiCl_4$ core-Shell catalyst for establishing structure-performance relationship in Ziegler-Natta olefin polymerization. Top Catal 57: 911-917
13. Poonpong S, Dwivedi S, Taniike T, Terano M (2014) Structure-performance relationship for dialkyldimethoxysilane as an external donor in stopped-flow propylene polymerization using a Ziegler-Natta catalyst. Macromol Chem Phys 215: 1721-1727
14. Barrett EP, Joyner LG, Halenda PH (1951) The determination of pore volume and area distributions in porous substances. I. Computations from nitrogen isotherms. J Am Chem Soc 73: 373-380
15. Innes WB (1957) Use of parallel plate model in calculation of pore size distribution. Anal Chem 29: 1069-1073
16. Tanase S, Katayama K, Inasawa S, Okada F, Yamaguchi Y, Konakazawa T, Junke T, Ishihara N (2008) Particle growth of magnesium alkoxide as a carrier material for polypropylene polymerization catalyst. Appl Catal A: Gen 350: 197-206
17. Sing KSW, Everett DH, Haul RAW, Moscou L, Pierotti RA, Rouquérol J, Siemieniewska T (1985) Physical and biophysical chemistry division commission on colloid and surface chemistry including catalysis. Pure Appl Chem 57: 603-619
18. Sing KSW (1982) Reporting physisorption data for gas/solid systems with special reference to the determination of surface area and porosity (Provisional). Pure Appl Chem 54: 2201-2218
19. Horvath G, Kawazoe K (1983) Method for the calculation of effective pore size distribution in molecular sieve carbon. J Chem Eng Japan 16: 470-475
20. Saito A, Foley HC (1995) Argon porosimetry of selected molecular sieves: experiments and examination of the adapted Horvath-Kawazoe model. Microporous Mater 3: 531-542
21. Taniike T, Chammingkwan P, Thang VQ, Funako T, Terano M (2012) Validation of BET specific surface area for heterogeneous Ziegler-Natta catalysts based on α_s-plot. Appl Catal A: Gen 437-438: 24-27